JOURNAL OF MATERIALS SCIENCE 21 (1986) 2269–2272

Adhesion of TiC and TiN coatings prepared by chemical vapour deposition on WC–Co-based cemented carbides

M. T. LAUGIER*
Materials Testing Laboratory, 9 Nova Croft, Coventry, Warwickshire CV5 7FJ, UK

Adhesion energies of CVD-prepared TiC and TiN coatings on WC–Co-based cemented carbides are determined on the basis of an energy formulation of the scratch test. Values found for the adhesion energy W are $W_{TiC} = 10\,J\,m^{-2}$ and $W_{TiN} = 46\,J\,m^{-2}$.

1. Introduction

Titanium nitride and titanium carbide layers in the thickness range 5 to 20 μm, produced by chemical vapour deposition (CVD), are used to provide increased wear resistance of cemented carbide cutting tools.

The effectiveness of a coating in enhancing cutting-tool wear resistance is generally assessed by means of controlled cutting tests. From a physical point of view, the effectiveness of any coating must be dependent on the degree of bonding between the coating and the substrate material.

Adhesion measurements have been made extensively over a number of years, mainly on thin films, using a variety of techniques, sometimes with conflicting results [1]. Although at present there is no generally accepted method for determining the adhesion of coatings, the scratch test has been used successfully in a number of investigations, and is probably the most versatile technique available. CVD coatings tend to be extremely adherent, and to the authors' knowledge can only be effectively removed using the scratch test. In this technique, a smoothly rounded probe is drawn across the coating under increasing normal loads and the critical load at which coating removal occurs is taken as a measure of adhesion.

The technique has suffered from difficulties of interpretation following scanning electron microscope (SEM) observations of the removal process which showed coating removal to be more complex than originally envisaged, and the mode of detachment has been found to depend on the coating material [2]. Explanations for the SEM observations have been provided [1, 3] and a dynamic model which includes the effects of friction has been developed [3]. Ductile coatings tend to fail by peeling, whereas brittle coatings tend to spall.

The scratch test has also been used as a measure of adhesion of CVD coatings by Perry [4] who investigated TiC and TiN coatings applied to steel substrates and by Hammer *et al.* [5] who investigated TiC coatings applied industrially, also to steel substrates.

2. Principle of the method

An energy criterion has recently been proposed for the onset of coating removal which is applicable to both ductile and brittle coating materials [6]. Debonding requires the application of an interfacial shear stress of a critical value, representative of the coating adhesion. However, coating removal will not occur unless the associated strain-energy release rate is at least equal to the work of adhesion.

Complete coating removal does not normally occur abruptly, indicating that, in general, a greater load is required for complete coating removal than is required to first exceed the shear strength of the interface. In cases where spontaneous stripping occurs at a critical load, without previous indication of failure, then the strength of the interface as measured by the critical interfacial shear stress would be the controlling factor.

In terms of a balance between the work of adhesion and the stored elastic energy in the coating in the region ahead of the indenter, the work of adhesion W is given [6] by the relation

$$W = \frac{\sigma^2}{2E} h$$

where h is the thickness of the coating, E is the Young's modulus of the coating and σ is the compressive stress in the coating ahead of the indenter.

The work of adhesion $W = \gamma_1 + \gamma_2 - \gamma_{12}$, where γ_1, γ_2 are the surface energies of the coating and the substrate and γ_{12} is the interfacial energy. The compressive stress σ ahead of the indenter is given by $\sigma = \sigma_{appl} + \sigma_{int}$, where σ_{appl} is the applied stress due to the moving indenter, and is determined by both the frictional properties of the coating/indenter interface, and the mechanical properties of the substrate, and σ_{int} is the internal stress in the coating, which may be compressive or tensile. CVD coatings are produced at temperatures in the region of 1000° C, and may develop substantial tensile thermal stresses on cooling. An expression for this differential contraction stress may be written

$$\sigma_{d.c.} = -\frac{E\Delta\alpha\Delta T}{(1-\nu)}$$

*Present address: Materials Research Centre, NIHE, Limerick, Ireland.

0022–2461/86 $03.00 + .12

where E is the Young's modulus of the coating, ν the Poisson's ratio of the coating, ΔT the temperature change and $\Delta\alpha$ the difference in coefficients of thermal expansion of the coating and the substrate. In the absence of reported experimental data, it is assumed that $\sigma_{int} \sim \sigma_{d.c.}$. This requires that $\sigma_{intrinstic} \ll \sigma_{d.c.}$, where $\sigma_{intrinsic}$ is that part of σ_{int} resulting from non-equilibrium effects arising during coating deposition. Since CVD is a slow, high-temperature process, the assumption $\sigma_{int} \sim \sigma_{d.c.}$ appears reasonable.

The compressive stress σ_{appl} may be written [3, 7]

$$\sigma_{appl} = \frac{P}{2\pi a^2}\left[(4 + \nu')\frac{3\pi f}{8} - (1 - 2\nu')\right]$$

$$= \frac{P}{a^2} F(f, \nu')$$

where a is the Hertz radius of contact [8] given by

$$a^3 = kPR/3E$$

where

$$k = \frac{9}{16}\left[(1 - \nu''^2) + (1 - \nu''^2)\frac{E'}{E''}\right]$$

Here P is the normal load applied to the indenter, R is the radius of curvature of the indenter, E', E'' and ν', ν'' are respectively the Young's moduli and Poisson's ratios of the substrate and the indenter, and f is the coefficient of friction between the indenter and the coating.

It is noted that within the confines of the present model, σ_{appl} should have a maximum value when $P/\pi a^2 = H$, the hardness of the softer material. However, greater values of σ_{appl} are possible if significant work-hardening occurs or if the effective coefficient of friction increases with load.

3. Experimental details

The scratch-test measurements were performed using simple apparatus similar to that of Benjamin and Weaver [9] using a diamond indenter of tip radius 100 μm. Commercially available cemented carbide cutting tips CVD-coated with TiN and TiC were lightly polished using 0 to 2 μm diamond paste before testing.* The coefficient of friction of the diamond sliding at about 10 mm min^{-1} was found to be close to 0.15 for both materials. Coating removal was readily detected using optical microscopy.

Microhardness measurements were made on both the coated cutting tips and on the cemented carbide substrates after grinding off the coating and polishing. Coatings were further characterized by optical microscopy and scanning electron microscopy (SEM) with energy-dispersive X-ray analysis (EDS), using a Cam Scan 3–30 ACV SEM with a Link Systems 860 Series 2 EDS analyser (Cambridge Scanning Co. Ltd. Cambridge, UK). Phase identification was performed by X-ray diffraction.

4. Coating characterization

Optical micrographs of sections through the TiN and TiC coatings, polished and etched for 2 min with Murakami's reagent (equal volumes of NaOH 20% w/v and $K_3Fe(CH)_6$ 20% w/v) are shown in Figs 1 and 2. The presence of an η-phase layer is clearly seen beneath the TiC coating in Fig. 2. The thickness of the TiN coating was 8 μm, that of the TiC coating was 4 μm and that of the η-phase region was about 6 μm.

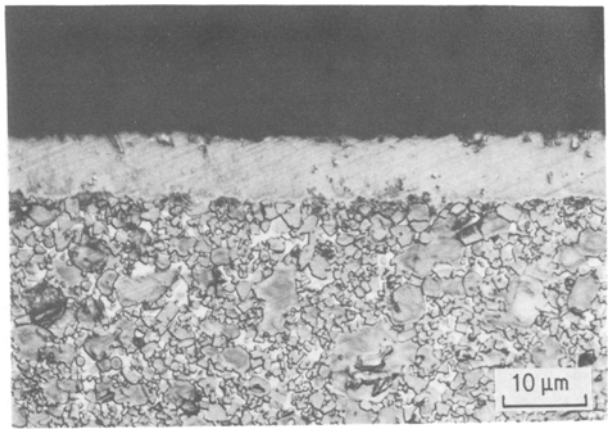

Figure 1 Optical micrograph of a polished and etched section through a TiN coating and the cemented carbide substrate.

SEM observations of TiC fracture surfaces showed the coatings to consist of submicrometre equiaxed grains decreasing in size towards the TiC/cemented carbide interface. A further notable feature was the frequent presence of interfacial cracks or voids, also seen in Fig. 3.

Fig. 4 is an SEM micrograph of a TiN fracture surface. Near the TiN/cemented carbide interface the coating appears to consist of submicrometre grains. A significant increase in grain size ($\gg 1$ μm) is observed on approaching the outer TiN surface, with a tendency to columnar morphology. Interfacial cracking was not observed in the case of TiN coatings. EDS did

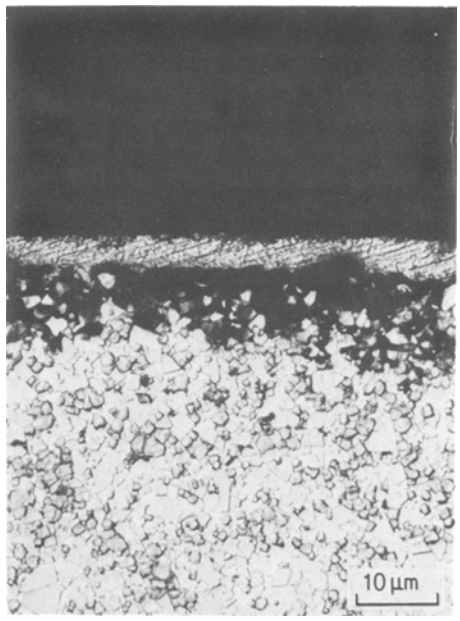

Figure 2 Optical micrograph of a polished and etched section through a TiC coating and the cemented carbide substrate. The dark region below the coating indicates carbon depletion.

*Edgar Allen ES20 TiN-coated substrate containing approximately 9 wt % Co, 15 wt % γ-carbides [(Ti, Ta, Nb) C] and 76 wt % WC; Wimet CW540 TiC-coated substrate containing approximately 11 wt % Co, 12 wt % γ-carbides [(Ti, Ta, Nb) C] and 77 wt % WC.

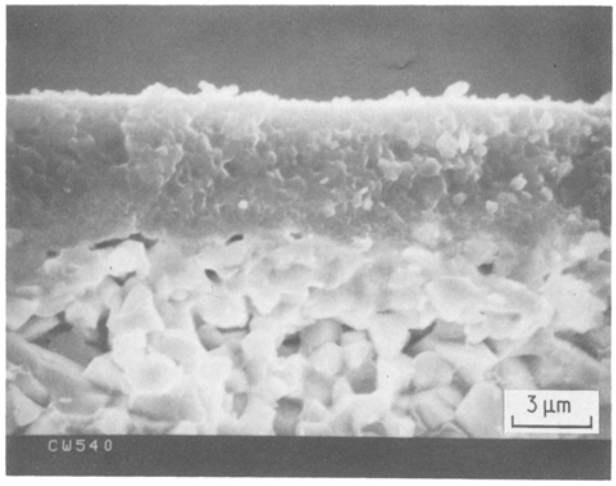

Figure 3 SEM micrograph of a TiC fracture surface. Cracks or voids are apparent at the TiC/cemented carbide interface.

not indicate the presence of tungsten or cobalt in any of the coatings. Only the main constituents of the TiC and TiN coatings could be identified by X-ray diffraction; the structure of the η-layer beneath the TiC coatings was found to be W_6Co_6C, in agreement with earlier findings discussed below.

The η-phase layer was first reported as W_6Co_6C by Sproul and Richman [10] and confirmation of this was provided by Sharma and Williams [11] using electron diffraction, and by Breval and Vuorinen [12] using X-ray diffraction. The η-phase layer is considered to result from the decarburizing conditions present during TiC deposition, which occurs at $\sim 1000°$ C in the presence of $TiCl_4$ and CH_4. Carbon required for the nucleating TiC layer is available by diffusion from the cobalt-rich binder phase (β-phase); the cubic γ carbides may also act as carbon sources [13].

Nucleation will be favoured on exposed γ carbides and in binder phase regions, leading to rapid grain growth and the production of a very fine initial TiC deposit.

The cobalt-rich binder can only coexist as a solid solution in equilibrium with WC in a very narrow phase field, owing to the high stoichiometry of WC; when carbon diffuses out of the binder, carbon-deficient regions transform to η-phase [14]. The highly

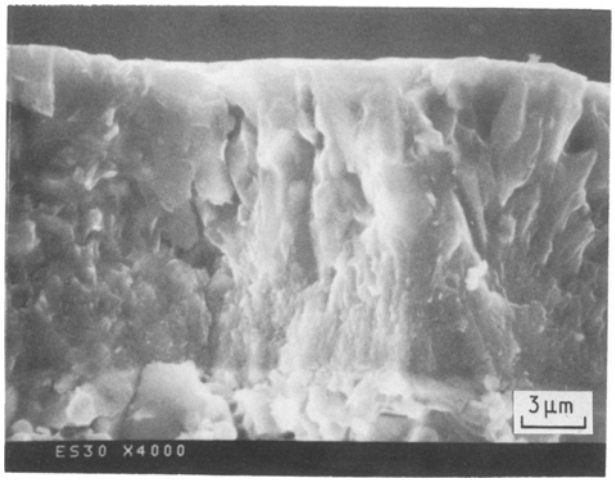

Figure 4 SEM micrograph of a TiN fracture surface, showing a thicker than usual TiN layer.

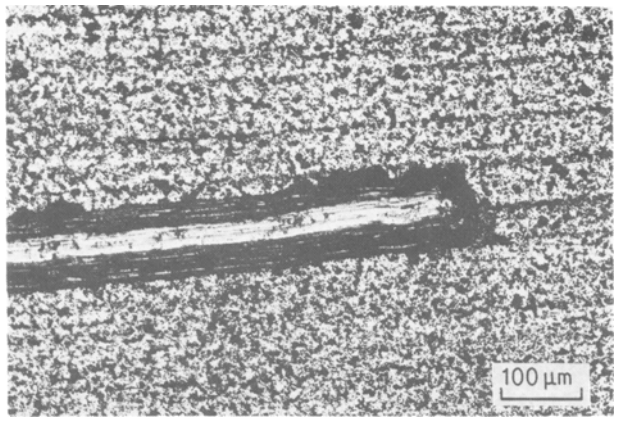

Figure 5 Optical micrograph of a typical scratch track on a TiN coating produced using a load of 2 kg. Direction of stylus movement was from left to right.

stoichiometric WC is unable to redress the carbon balance by liberating carbon. The need for critical control of carbon is well known in the cemented carbide industry; carbon imbalances of 0.10% can lead to the precipitation of graphite or η-phase for excess or deficiency of carbon, respectively.

Recent transmission electron microscopy work of Vuorinen and Horsewell [15] has identified seven sub-interfaces of total thickness $\sim 0.5\,\mu$m associated with the TiC–cemented carbide interface, the structure and distribution of which they consider important determinants of adherence, wear properties and nucleation and growth of the TiC layer.

Using a 200 g load, microhardness values of 19.6 and 13.7 GPa were obtained for the TiC coating and the substrate, respectively, and 18.2 and 17.2 GPa for the TiN coating and the substrate, respectively.

5. Scratch test results

Coating removal occurred by spalling ahead and to the side of the indenter. Figs 5 and 6 show typical scratch tracks on TiN and TiC layers. Complete removal of the coatings has occurred along the centre of the track, indicating critical loading conditions. The critical loads were 2.0 kg for TiN and 0.8 kg for TiC.

The scratch track widths measured over the central regions of complete coating removal were only about

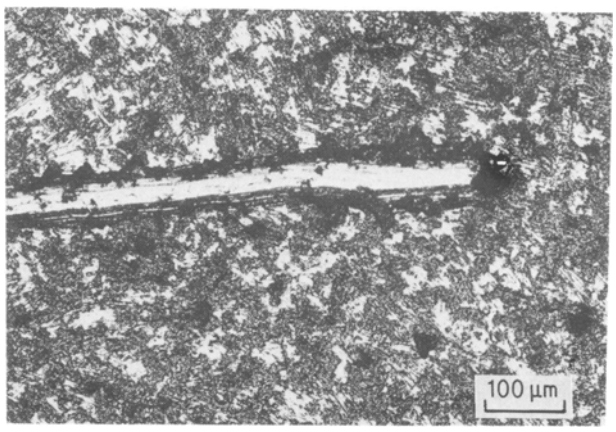

Figure 6 Optical micrograph of a typical scratch track on a TiC coating produced using a load of 0.8 kg. Direction of stylus movement was from left to right.

TABLE I Mechanical and thermal data [16].

Material	Poisson's ratio, ν	Young's Modulus, E (10^5 MPa)	Coefficient of thermal expansion, $\alpha(10^{-6}\,K^{-1})$
WC–Co	0.25	6.0	5.0
TiN	0.25	2.5	9.3
TiC	0.25	3.2	7.4
Diamond	0.20	10.5	

10% greater than the calculated values, using Hertzian theory of 31 μm for TiN and 23 μm for TiC, although the overall width of the spalled regions was considerably greater, as can be seen from Figs 1 and 2.

The compressive critical applied stresses calculated from the formulae given earlier are $\sigma_{appl}(TiC) = 2300\,MPa$ and $\sigma_{appl}(TiN) = 3100\,MPa$. Similarly the thermally generated tensile stresses in the coatings calculated from the formulae are $\sigma_{int}(TiN) = 1400\,MPa$ and $\sigma_{int}(TiC) = 1000\,MPa$. The mechanical and thermal data required, taken from published tables [16], are given in Table I.

The resultant compressive stress in the coating ahead of the indenter is given by $\sigma = \sigma_{appl} + \sigma_{int}$. For TiC the critical resultant stress $\sigma = 1300\,MPa$ and for TiN, $\sigma = 1700\,MPA$. Using these values in the formula for the adhesion energy W gives $W_{TiC} = 10\,J\,m^{-2}$ and $W_{TiN} = 46\,J\,m^{-2}$.

6. Discussion

It is of interest to note that good adhesion of a similar order to that observed in CVD coatings has also been found in thin films of iron, chromium, titanium, molybdenum, magnesium and zirconium vacuum-evaporated at normal ambient temperatures on to glass substrates [17]. The high values of adhesion in these cases have been attributed to oxide formation at the film/substrate interface, and the adhesion energy calculated for the case of iron was $3.8\,J\,m^{-2}$ (2.4 eV bond^{-1}).

The present very high values of adhesion energies may again be qualitatively understood on the basis of chemical bonding, which has been demonstrated in the case of TiC coatings (see Section 4). The detailed nature of the TiN/cemented carbide interface has not been investigated in detail. The SEM observations of frequent interfacial fractures in the case of TiC coatings, which were not observed with TiN coatings, illustrates the greater brittleness of TiC coatings and is consistent with the lower fracture surface energy and the lower critical interfacial shear stress observed in TiC.

For a discussion of the results of Perry [4] and of Hammer *et al.*, [5] it is convenient to write the results of the present model in the form

$$P = \beta \frac{W^{3/2}}{H^{1/2}} \frac{1}{h^{3/2}} \frac{1}{F(f, \nu')} \left[1 + \frac{\sigma_{int}}{\sigma_{appl}}\right]^{-3} R^2$$

where β is a constant. It is emphasised that this model assumes elastic behaviour and requires $a \gg h$. In the work of Perry [4] and Hammer *et al.* [5] steel substrates were used, and significant plastic deformation occurred in both cases. However, they found a tendency for the critical load P to increase with both substrate hardness H and coating thickness h, in contrast to the predictions of the model. They used diamond indenters of radius $R = 200\,\mu m$, and since P scales with R^2, the present results extrapolated for an indenter with $R = 200\,\mu m$ become 3.2 kg for TiC and 8.0 kg for TiN coatings. These results are quite similar to those of the earlier workers.

The observation that measured scratch track widths were only about 10% greater than values calculated from Hertzian theory suggests that plastic deformation was relatively slight. On the basis of this result it is of interest to calculate the contact pressures at the critical applied loads for coating removal. These are 19.5 GPa in the case of TiC and 26.4 GPa in the case of TiN; these values compare with hardnesses of 13.7 GPa and 17.2 GPa for the respective substrates, and suggest that considerable work-hardening has taken place.

Acknowledgement

Experimental work was performed whilst the author was with Sandvik Hard Materials UK Research Centre.

References

1. C. WEAVER, *J. Vac. Sci. Technol.* **12** (1975) 18.
2. D. W. BUTLER, C. T. H. STODDART and P. R. STUART, *J. Phys. D* **3** (1970) 877.
3. M. T. LAUGIER, *Thin Solid Films* **76** (1981) 289.
4. A. J. PERRY, *ibid.* **81** (1981) 357.
5. B. HAMMER, A. J. PERRY, P. LAENG and P. A. STEINMANN, *ibid.* **96** (1982) 45.
6. M. T. LAUGIER, *ibid.* **117** (1984) 243.
7. G. M. HAMILTON and L. E. GOODMAN, *J. Appl. Mech.* **33** (1966) 371.
8. S. TIMOSHENKO and J. N. GOODIER, "Theory of Elasticity" (McGraw-Hill, New York, 1951).
9. P. BENJAMIN and C. WEAVER, *Proc. R. Soc.* **A254** (1960) 163.
10. W. D. SPROUL and M. H. RICHMAN, *J. Vac. Sci. Technol.* **12** (1975) 842.
11. N. K. SHARMA and W. S. WILLIAMS, *J. Amer. Ceram. Soc.* **62** (1979) 193.
12. E. BREVAL and S. VUORINEN, *Mater. Sci. Eng.* **42** (1980) 361.
13. N. K. SHARMA, W. S. WILLIAMS and R. GOTTSCHALL, *Thin Solid Films* **45** (1977) 262.
14. B. UHRENIUS, B. CARLSSON and T. FRANZEN, *Scand. J. Metall.* **5** (1976) 49.
15. S. VUORINEN and A. HORSEWELL, *J. Mater. Sci.* **17** (1982) 589.
16. P. K. PHILIP, *Wear* **47** (1978) 45.
17. P. BENJAMIN and C. WEAVER, *Proc. R. Soc.* **A261** (1961) 516.

Received 4 July
and accepted 8 August 1985